SLOVAK UNIVERSITY OF TECHNOLOGY IN BRATISLAVA
Faculty of Civil Engineering

Ing. Jana Čepčianska

Dissertation Thesis Abstract

Material Composition and Properties of Fibre-Reinforced Heavy-Weight Self-Compacting Concretes

to obtain the Academic Title o f„philosophiae doctor“, abbreviated as „PhD“.
in the doctorate degree study programme D-TS4. Building Technology

and

in the field of study: Civil Engineering

Form of Study: full-time study

Bratislava 2024

STU

Dissertation Thesis has been prepared at Institute of Construction and Architecture Slovak Academy of Sciences

Submitter: Ing. Jana Čepčianska
Department of Structures and Materials
Institute of Construction and Architecture
Slovak Academy of Sciences
Dúbravská cesta 9, 845 03 Bratislava 45

Supervisor: prof. Dr. Ing. Martin Tchingnabé Palou
Department of Structures and Materials
Institute of Construction and Architecture
Dúbravská cesta 9, 845 03 Bratislava 45

Consultant: Ing. Matúš Žemlička, PhD.
Department of Structures and Materials
Institute of Construction and Architecture
Slovak Academy of Sciences
Dúbravská cesta 9, 845 03 Bratislava 45

Dissertation Thesis Abstract was sent: 22. 07. 2024

Dissertation Thesis Defence will be held on ..09. 2024 *at*.....*(am/pm) at* ***Faculty of Civil Engineering, SUT Bratislava,*** *Radlinského 11, 810 05 Bratislava*

prof. Ing. Stanislav Unčík, PhD.

Introduction

Self-compacting concrete (SCC) represents a modern building material possessing specific properties. In addition to self-consolidation, SCC possesses rheological characteristics predisposing them to use in constructions requiring good flowability, permeability through densely reinforced areas, resistance to the segregation of components, or pumping ability [1, 2]. To accomplish this objective, it is imperative to incorporate plasticizing or water-reducing additives. Plasticizing additives provide consistency, and stability as well as reduce the water coefficient, positively affecting the strength characteristics of the hardened concrete [3].

Heavy-weight self-compacting concretes (HWSCC) represent composites possessing SCC characteristics, also characterized by a bulk density exceeding 2,600 kg m^{-3}. This type of concrete employs natural or synthetic heavy-weight aggregates with a bulk density of over 3,000 kg m^{-3}. Due to the physical characteristics of heavy-weight aggregates employed in this type of concrete, heavy-weight concretes significantly contribute to the shielding of ionizing radiation at nuclear power plant sites, and radioactive waste storage areas [4, 5]. An important aspect of the shielding concretes is their homogeneity. In the case of the HWSCC, the heavy-weight aggregate tends to segregate. For this purpose, attention should be paid to selecting a suitable technology for the construction of the considered structures [6].

Fiber-reinforced heavy-weight self-compacting-concrete (FRHWSCC) prepared and studied in this dissertation thesis represents an innovative composite material combining the properties of self-compacting concrete (self-compacting, flowability, passing ability, etc.), heavy-weight concrete (high bulk density, shielding ability, etc.), and fiber-reinforced concrete (flexural and post-crack behavior, etc.). The incorporation of fibers, and the formation of a bond between the concrete matrix, and the fibers results in a material with enhanced mechanical characteristics, including ductility, toughness, stiffness, and slower crack propagation [7]. For this thesis, polypropylene (PP), multi-walled carbon nanotubes (CNT), and steel (S) fibers were employed.

In addition to the above-mentioned components, supplementary cementitious materials (SCMs) including ground-granulated blast-furnace slag (GGBFS), grounded limestone (GL), and metakaolin (MK) were also employed in this work. Depending on the substitution level, SCMs exhibit no adverse impact on the final mechanical properties of concrete. On the contrary, SCMs can improve the workability of fresh concrete mixtures, and the durability of hardened concrete [8].

1. Actual state of the art

1.1. Self-compacting concrete

In recent years, there has been a growing interest in producing sustainable building materials, and the effective management of construction and demolition waste. By incorporating recycled raw materials, specifically aggregates, into the concrete production process, it is possible to reduce the pressure on extracting natural raw materials. Numerous studies have examined the substitution of natural aggregates (NA) by recycled aggregates (RA) in SCC mixes, regardless of the coarse or fine aggregates [9- 11]. However, many challenges are associated with using RA, including its composition, potential contaminants, particle shape, compatibility with cementitious materials, and shrinkage properties.

It is possible to mention the workability of the fresh-state properties, fundamentally distinguishing SCC from conventional vibrated concrete. According to Campos et al. [12], a greater quantity of superplasticizers (SP) was employed in the design of SCC mixtures containing either 20 mass% fine RA or 20 mass% coarse RA in comparison to SCC with NA. The quantity of SP increased in proportion to the RA content, and it was also observed that the water absorption of RA was higher than that of NA.

Compressive strength can be mentioned as one of the important properties of hardened concrete. Fiol et al. [13] reported that with 50 to 100 mass% NA replacement, RA concrete mixtures would achieve higher compressive strengths than a referential sample. Furthermore, when NA was 100 % replaced, the compressive strength was 16 % higher. The reason for this is the higher water absorption of RA, and at the same w/b ratio caused a higher increase in the strength. However, according to Manzi et al. [14] the incorporation of fine RA in quantities below 20 mass% results in an unpredictable development of the compressive strength.

1.2. Heavy-weight concrete

With the expansion of nuclear laboratories, nuclear waste storage facilities, as well as nuclear power plants, new challenges have arisen, requiring increased HWC consumption, leading to increased materials costs. Besides finding economically more available constituent materials for HWC, these challenges include increasing the insulating abilities of existing materials against gamma, neutron, and X-ray radiation penetration.

In addition to increasing the percentage of heavy-weight aggregate, other possibilities have arisen such as the use of PP fibres. Martínez-Barrera et al. [15] examined the impact of gamma radiation on the characteristics of samples comprised of OPC, silica sand particles (fraction size of 150 μm), marble (fraction size of 1.4 and 9.5 mm), and with a cement/aggregate component ratio of 1/2.75,

and a w/b ratio of 0.485. These samples were further incorporated by atactic PP fibres of length 10 mm, and diameter 30 – 40 μm at 1.0, 1.5, or 2.0 vol. %. The study concluded that gamma-irradiated samples displayed higher compressive strength and compressive modulus in comparison to non-irradiated reference samples. However, the extent of this improvement depends on the radiation dose, the number of PP fibers, and the size of the marble particles. The ionization energy of gamma radiation up to 50 kGy increases surface contact between the hydrated cement phase and the other components. Nonetheless, by employing higher doses of this radiation (100 kGy), a greater quantity of disintegrated marble particles and surface defects were observed in the samples on PP fibers [16]. The design and function of containers for nuclear waste repositories not only impose significant demands on the shielding capabilities of HWC but also on the strength and durability of the concrete employed. A study led by Tufekci and Gokce [17] investigated high-performance fiber-reinforced concretes (HPFRC) containing baryte aggregate and GFW with different w/b ratios (0.18, 0.24, and 0.36), and steel fiber fractions (1, 2 and 3 %) under standard and steam curing regimes. The results of the study showed that the GFW HPFRC obtained the best values of linear attenuation coefficient μ for gamma radiation with an energy of 0.662, and 1.250 MeV, respectively. The baryte samples have achieved the highest value of this coefficient for radiation with an energy of 0.200 MeV. As the w/b ratios in mixtures increased from 0.18 to 0.36, there was a consistent rise in μ for both types of aggregates studied. However, it has not been proven that the type of curing regime has a major impact on μ.

1.3. Fiber-reinforced concrete

The addition of fibers [18], geopolymers in the form of binder admixtures [19], or minerals admixtures [20] are frequently used methods to enhance crack resistance by improving ductility, and tensile strength, and reducing shrinkage, as well. Currently, the extent of the impact of fiber properties, e.g. strength, shape, or modulus of elasticity, on the characteristics of the final concrete remains a subject of debate [21]. This claim is supported by the numerous studies focused on using steel fibers [22-25]. Based on the mentioned studies can be concluded that end-hooked and arched steel fibers possess the highest potential for enhancing compressive, tensile, and flexural properties. Regarding the size of steel fibers, studies have indicated a high aspect ratio can enhance compressive and tensile strength [26], in addition to the bending resistance [27]. However, an aspect ratio above 100 significantly reduces the workability of the fresh mixture and leads to problematic concrete placement [27].

In recent decades, interest in PP fibers has increased primarily due to economic availability. Advantages of PP fibers include an increase in the impact resistance

of concrete, while at 0.4 to 1.2 % content, the dynamic properties can be improved [28]. Due to the high specific surface area of PP fibers, the formation of microcracks is reduced. However, the use of separate PP fibers has a weak effect on the compressive strength development [29, 30].
Other commonly used fibers including microfibres possess the capability to bridge micro-cracks, thereby reducing the occurrence of micro-defects, as opposed to macro-fibers. Specifically, carbon nanotubes (CNTs) and various types of whiskers are currently being discussed. The study by Cui et al. [31] focusing on the effect of 12 types of multi-walled carbon nanotubes (MWCNTs) on the mechanical properties of cementitious composites, can be mentioned. The contents of MCWNTs in the samples were 0.0, 0.1, 0.5, and 0.8 %. The study demonstrates that the diameter of MWCNTs has a significant impact on the strength development of the samples, with the largest increase in compressive strength of 47 % and flexural strength of 55 % observed in samples containing 0.1 % of short (0.5 – 2 μm), and large-diameter (20 – 30 nm) MWCNTs.

1.4. Fiber-reinforced heavy-weight self-compacting concrete

There are very few studies focusing on this type of concrete, among which the work of Aslani et al. [32] can be mentioned. The study is aimed at evaluating the fresh and mechanical properties of two series of FRHWSCC with OPC replacement by 25.7 mass% of FA, 17.2 mass% of GGBFS, 7.5 mass% GL, and 0.6 mass% of SF with a w/b ratio of 0.45. In series I, 75 mass% of the coarse and fine normal-weight aggregates (NWA) were replaced with magnetite aggregates. In series II, only magnetite aggregate was used. Series I comprised four samples containing steel fibers of 0.25, 0.5, 0.75, and 1.00 vol. %. The other four samples contained PP fibers of 0.10, 0.15, 0.20, and 0.25 vol. %, respectively. In both series, different concentrations of viscosity-modifying admixtures, superplasticizers, and high-range water-reducing agents were used.
The experimental results indicate that fibers and magnetite aggregates used with higher absorption than NWA deteriorated the flowability of fresh SCC mixtures. The high specific surface area of PP and the ability of steel fibers to trap particles during flow increased the viscosity of the mixtures. Nevertheless, in general, mixtures containing steel fibers exhibited enhanced passing ability. In terms of flowability, PP mixtures demonstrated better properties owing to the elastic nature of the fibers.
The bulk density of hardened mixtures including 100 mass% magnetite aggregate showed values exceeding 2,600 kg m^{-3}, whereas mixtures containing NWA replacements did not surpass this value. This finding is supported by the increase in air content and void space through the addition of the fibers.
The samples with a 75 mass% magnetite aggregate content reached a lower compressive strength than the samples with 100 mass%. The addition of 0.75 %

steel fibers, and 0.25 % polypropylene fibers increased 7- and 28-day strengths compared to the control sample without fibers.
The tensile strength determination revealed that increasing magnetite content decreases the tensile strength, whereas the incorporation of fibers enhances this strength. However, this occurrence was observed only in the samples with a greater than 0.75 % steel fiber content. In the samples with lower contents, the tensile strength decreased due to the voids in the cement paste formed by the addition of steel fibers. Regarding PP fibers, increasing their content also increased tensile strength. The sample containing 0.25 % PP fibers in both series exhibited the highest tensile strength values.
However, this work encourages further research to establish toughness indices, and residual strength factors for a more precise evaluation of the post-cracking behavior of FRHWSCC.

2. Materials and sample preparation

The experimental part was focused on a set of 32 different FRHWSCC mixtures through different variables including the replacing level of OPC, aggregate, and fiber type. The subsequent components – binder, aggregates, and mixing water were used in a mass ratio of 1:3.25:0.42 in baryte samples, and 1:3.8:0.42 in magnetite samples.
The samples were categorized into 4 distinct series, specifically S100, S85, S80, and S65. Each series consists of 8 samples, of which 4 include baryte aggregate, and 4 include magnetite aggregate. In each of these sample quartets, separate PP fibers, CNTs, and straight S fibers were employed. The fiber-free sample served as a reference in determining the influence of the fibers on the observed characteristics.
In the S100 series, pure OPC was employed, and this series served as a reference for evaluating the impact of SCMs on individual characteristics. The S85 series contained 15 mass% of GGBFS, whereas the S80 series contained a 15 mass% of GGBFS and 5 mass% of MK. Additionally, the S65 series used SCMs to replace OPC up to 35 mass%, specifically 15 mass% of GGBFS, 15 mass% of GL, and 5 mass% of MK. Furthermore, polycarboxylate plasticizing additive STM 910 (density 1,050 ± 20 kg m^{-3}), and the synthetic copolymer-based stabilizing additive to reduce water segregation, Stabilan KC 0.3 (density 1,000 ± 20 kg m^{-3}), were used to optimize the rheological characteristics of samples. The dosage of additives (**Tab. 1-1**) is related to the mass of the binder mixtures employed in particular series S100 – S65.
The grain size composition of both aggregate types was set to obtain grading curves of aggregates with a maximum grain size of 2 mm. Based on Fuller´s curve, a grading curve for the used aggregates was constructed (**Fig. 1-1**).

Tab. 1-1. The dosage of superplasticizer (SP) and stabilization additive (SA).

Additive	SP/ mass%				SA/ mass%			
Sample	**S100**	**S85**	**S80**	**S65**	**S100**	**S85**	**S80**	**S65**
B	0.8	0.7	1.0	0.9	0.10	0.10	0.10	0.10
B-PP	1.7	1.5	2.1	1.8	0.10	0.10	0.10	0.10
B-CNT	1.0	0.9	1.2	1.1	0.40	0.40	0.20	0.50
B-S	0.9	0.8	1.2	1.0	0.40	0.30	0.10	0.50
M	1.7	1.5	2.2	1.9	0.80	0.95	1.00	0.95
M-PP	3.7	3.3	4.5	3.9	1.00	0.70	0.60	1.00
M-CNT	1.8	1.2	2.5	2.3	0.80	0.60	0.80	0.95
M-S	2.0	1.7	2.3	2.1	0.95	0.60	0.60	0.95

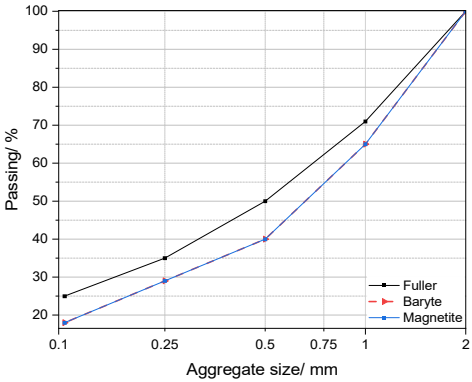

Fig. 1-1. Grading curves of aggregate used.

The preparation of the samples was carried out following the STN EN 1015-11 for mortars [33], STN EN 206/NA [34], and the European guidelines for SCC [1, 2]. The fresh concrete mixtures were poured into the prism molds (40 x 40 x 160 mm^3). Molds were subsequently covered with moist fabric, and plastic foil to avoid evaporation of surface water. Mixtures were left to hydrate at an ambient temperature for the first 24 hours. Solidified samples for bulk density, compressive and, flexural tensile strength determination were de-moulded, and submitted to the standard curing conditions for 2, 7, 28, 90, 180, and 365 days. The samples used for the shrinkage characteristics determination were cured in a dry climatic chamber (r. h. 30 %, *t* 24 ± 1 °C). Referential OPC, as well as blended mixtures for thermal and high-temperature X-ray powder diffraction analysis, were prepared separately by mixing the dry binder with the addition of an adequate amount of water, and chemical additives.

3. Methods

Binder materials characterization:
air permeability Blaine method, gas adsorption analysis, standard consistency test, and setting time determination.
Aggregate properties characterization:
bulk density determination, and gas adsorption analysis.
Rheological properties of the fresh concrete:
mini slump-flow test, time T_{200}, visual stability index determination, and mini V-funnel test.
Physicomechanical properties of the hardened concrete:
thermal analysis and high-temperature X-ray powder diffraction analysis, bulk density determination, flexural tensile strength and stiffness determination, compressive strength and shrinkage characteristics determination, mercury intrusion porosimetry, and scanning electron microscopy.

4. Results and discussion

4.1. Standard consistency, and setting time determination

The setting time as depicted in was determined in OPC paste and blended binder pastes. From the obtained results, it can be concluded that the specific surface area of individual components and their synergistic effect influence the setting time. A material with a higher specific surface area provides a larger contact with water, thereby enhancing its reactivity [35]. An increase in reactivity leads to a faster loss of plasticity, and reduced workability of the paste [36].
The ternary blended mixture S80 exhibited the highest specific surface area among the other binders, thus exhibiting the lowest workability rate (60 min).
In contrast, the workability of the two-component blended mixture S85 containing OPC and GL, with the lowest specific surface area, was found to be the longest (325 min). This is attributable to the substitution of OPC with a specific surface area of 1,456 $m^2\ kg^{-1}$ by 15 mass% of GL with a specific surface area of 709 $m^2\ kg^{-1}$, improving the workability of the blends [37]. Thus, in comparison to sample S100, there was a decrease of 11.5 % in the specific surface area. The workability of the four-component mixture S65 was 15 min longer than that of the S100 (300 min).

4.2. The rheological properties of fresh-state concrete

The sample mixtures were optimized to meet mini slump-flow test target requirements of 240 to 260 mm, T_{200} time requirements of 1 to 2.4 s, and mini V-funnel flow time requirements of 7 to 11 s [1] while maintaining a constant w/b ratio of 0.42.

As shown in **Tab. 1-1**, a higher concentration of additives was required in the magnetite mixtures. One of the possible reasons was the higher ratio of components in magnetite mixtures of 1:3.8:0.42 compared to the baryte mixtures of 1:3.25:0.42, and the higher specific surface area as well as wettability of the particular magnetite fractions used.
According to several studies, adding fibers generally deteriorates the flowability of a mixture by increasing the air content [38, 39]. This effect has been observed in PP-containing samples, as indicated by using the highest concentration of additives compared to other mixtures.
Regarding the SCMs influence, based on the study by V. Fonseca [40], mineral additives increase the viscosity of the mixtures owing to their higher specific surface area. To obtain optimal rheological parameters, the S85 – S65 series mixtures were modified with a higher additive dosage compared to the S100.
The spill diameters of the prepared mixtures varied between 240 and 260 mm, and the time T_{200} varied between 1.5 and 2.4 s. The flow time ranged between 6.1 and 10.8 s. The visual assessment of the mixtures during the slump-flow test varied from 0 to 1 VSI index. Therefore, all the prepared samples fulfilled the SCC requirements established by the EFNARC guidelines [1, 2].
Regarding the flowability assessed by the V-funnel test, the highest flowability was observed for the samples from each series as follows: for the S100 series, B-PP and M-CNT samples; for the S85 series, the B-CNT, M, M-PP, and M-S samples; and the S80 series, the B and B-S samples. From the S65 series, the highest flowability was observed in samples B and M. The visual evaluation of the samples revealed a high degree of stability, with no evidence of segregation of components or water separation. Although the samples containing PP and S fibers did not exhibit segregation of the components, slight bleeding was observed in the form of a slightly sheeny surface of the samples.

4.3. Hardened concrete properties

4.3.1. Thermal analysis, and high-temperature X-ray diffraction

The addition of SCMs to the initial mixtures led to changes in the amount, and the type of hydration products. A high-temperature X-ray powder diffraction (HT-XRPD) technique was used to better understand the poorly crystalline phases, which were formed during the hydration course. The particular temperatures were selected based on the results of DTG curves According to HT-XRPD, the first DTG shoulder in the case of S100 samples, which turns to the peak with the maximum at 72 °C in the case of S65 samples can be attributed to the decomposition of AFt phases (ettringite $C_3A_3C\bar{S}H_{32}$ in the case of S100, as well as carbonated ettringite $C_3A_3C\bar{C}H_{32}$, where sulfates were partially or fully substituted by carbonates in the case of S65 [41], and calcium hemicarboaluminate ($Ca_4Al_2O_{6.5}(CO_3)_{0.5}\cdot 12H_2O$), as

well. The subsequent DTG peak at about 106 °C can be attributed to the decomposition of poorly crystalline C-S-H gels, and calcium monocarboaluminate ($CaO{\cdot}Al_2O_3{\cdot}CaCO_3{\cdot}11H_2O$), which well corresponds to the disappearing of calcium monocarboaluminate pattern at a temperature of 135 °C on the HT-XRPD. The peak is bigger in the case of the S100 samples than the same peak in the case of the S65 samples. This fact results from a lower initial portion of OPC. In both cases, S100, and S65 samples, the maxima located at about 154 °C can be assigned to low crystalline C-A-S-H gels, and strätlingite (C_2ASH_8) [42, 43]. The very small shoulder on DTG curves at about 210 °C can be assigned to the decomposition of C_4AH_{13} [44, 45]. According to Song et al., the DTG peaks that lay at about temperatures of 246 °C, and 358 °C can be attributed to the 2-step decomposition of hydrogarnet (C_3AH_6) [46]. The DTG peak located at 450 °C belongs to portlandite [47]. In the case of a blended sample, the total amount of CH was decreased by two consequences. The first has origin in a lower initial amount of OPC, and the second one plays the role of a substrate in alkali-activating, and/or pozzolan reactions [48]. In both instances, the last DTG peak is attributed to the decomposition of $C\bar{C}$, which occurred at 730 °C for the S65 sample, and at 675 °C for the S100 sample, respectively. The difference in the maximum temperature can be assigned to $C\bar{C}$ origin [49]. It is also important to consider the influence of the initial GL portion on S65 composites.

4.3.2. Bulk density

As per STN EN 206/NA [34], concrete with a bulk density greater than 2,600 kg m^{-3} is classified as heavy-weight and can be considered a suitable candidate for shielding concrete. All of the prepared FRHWSCCs exceeded this bulk density threshold and can be considered as heavy-weight concretes. Furthermore, an increase in bulk density was observed in all the magnetite and baryte samples with curing time. This increase can be attributed to the formation of hydration products in the binder mixtures. These poorly crystalline or even more amorphous products penetrate the cement matrix, leading to a denser composite structure. In addition, the bulk density of the hydration products is expected to be higher compared to non-hydrated binders [50]. Additionally, the compressive strength of the samples increased during the hydration process. The lowest bulk density observed among the baryte samples was 2,658 kg m^{-3} (S100 B-PP after 2 days of treatment), while the highest value was observed at 3,179 kg m^{-3} (S85 B-S at 365 days of age).

The magnetite samples showed a significant increase in bulk density values from initial to annual dates, surpassing the classification limit with a minimum bulk density value of 3,350 kg m^{-3} (S65 M-PP after 2 days of curing). The highest bulk density value of 3,653 kg m^{-3} was noted when steel fibers were used, particularly

for sample S80 M-S after 365 days. It is concluded that the magnetite aggregate demonstrated improved performance regarding its impact on the bulk density.

4.3.3. Flexural tensile strength and load-deflection curves

The flexural tensile behavior of fiber-reinforced concrete is primarily influenced by the capacity of the fibers bridging a crack in the matrix to transfer stress across the crack. The steel fibers exert a bridging mechanism to bridge the formed tensile flexural crack. In this manner, there is space for the occurrence of post-cracking or residual strength, causing the sample to remain cohesive even after the crack has formed. However, the effect also depends on the length or slenderness of the fibers. Increasing the length, and slenderness of the fibers increases the post-cracking strength across the entire cross-section. This claim was formulated by Cominoli et al. [51] indicating that shorter fibers exhibit greater susceptibility to being pulled out of the cementitious sealant when subjected to force, consequently decreasing the stiffness of the composite. The above-described effect was also noted in the 6 mm long steel fiber-containing samples when the fibers were pulled out by the action of flexural tensile force. However, due to the utilization of a single fiber length in this thesis, it was not feasible to assess the rate of pull-out. Additionally, it was possible to determine that PP fibers with a length of 12 mm experienced a lower tearing rate due to their elasticity. Conversely, owing to their wider dispersion in the samples and relatively lower strength, PP fibers were torn significantly faster. Regarding the behavior of the CNTs, these fibers did not exhibit any impact on the crack bridging.

Regarding the effect of aggregates, magnetite samples demonstrated a positive impact on flexural tensile strength. After 28, 90, 180, and 365 days of curing, the values of these samples showed in all the series a range of 9.2 – 11.3 MPa, 9.5 – 12.3 MPa, 10.3 – 13.5 MPa, and 10.9 – 13.8 MPa, respectively. On the identical dates, the values of flexural tensile strength of the baryte samples vary between 5.3 – 9.2 MPa, 6.3 – 9.4 MPa, 6.9 – 10.7 MPa, and 7.9 – 11.3 MPa, respectively. In addition, the influence of SCMs was also evident. SCMs positively affected the strength development in most of the samples, specifically a combination of 85 mass% OPC and 15 mass% of GGBFS in the series S85 had the most significant impact on the long-term strengths in the majority of the samples. However, the influence of SCMs on short-term strengths was more difficult to define.

The load-deflection curves of samples from the series S100 and S65 indicated that during the initial loading (pre-peak) stage, the samples exhibited elastic behavior and with the increase in applied load, the deflection increased essentially linearly. As the applied load increased, the deflection increased essentially linearly. After the failure of the sample at the maximum load, the load for the samples without fibers decreased rapidly, resulting in a vertical drop observed in the curve. This drop

indicated a decrease in residual flexural stiffness. At this point, the sample lost bearing capacity.
However, in the PP, and S fibers samples, after reaching the maximum load, the applied force decreased, and deflection continued to increase due to the action of fibers. Consequently, it was possible to observe a post-peak curve demonstrating the pseudo-plastic behavior of samples. Therefore, the complete failure of the sample from crack initiation took longer due to the fiber resistance. The results further demonstrate the different post-peak curves depending on fiber type. The post-peak curves for samples with PP fibers demonstrated a vertical drop of up to 90 % of the maximum load. At this point, the load was relatively stable and the deflection of the sample increased until complete failure.
When steel fibers were used, the post-peak behavior of the samples displayed a greater degree of variability. However, all the steel fiber samples exhibit a common feature: after crack initiation at maximum load, there was a drop in the load, although it was not as pronounced as in the samples containing PP fibers. Additionally, a concave load-deflection curve could be observed until the samples fully collapsed.
Based on the load-deflection results, the maximum loads for the baryte samples were lower than those for the magnetite samples. This is consistent with the previously discussed bulk density, and flexural tensile strength development. Regarding the SCMs used, identifying a distinct trend in their impact on the deflection of the samples remains ambiguous.

4.3.4. Compressive strength

Compressive strength values varied depending on the type of aggregate, fibers, and SCMs used. The impact of aggregate type was evident, the magnetite samples demonstrated significantly higher strengths compared to the baryte samples from the initial dates to the long-term ones. This result is supported by the higher content of magnetite aggregate in the samples, its tougher structure, or grain shape [52].

The highest compressive strengths in most of the samples were observed using S fibers and controversially, the lowest compressive strength with the use of PP fibers, which were primarily used to improve flexural properties. The significant decrease in strength observed in these samples is attributed to their comprehensive structure. The reduced adhesion of the fibers to other components of the concrete mixture, and the addition of fibers resulted in the aeration of the composite matrix [53].
The steel fiber samples showed the highest strengths, which is consistent with the findings from [15, 21]. Compressive strength development upon the addition of CNTs was slightly lower compared to the reference samples without fiber addition. This may be attributed to their high dosage of 0.5 vol. % in the studied mixtures.

Another important factor in the prepared FRHWSCC is the use of SCMs. Their positive effect was observed in all the baryte samples in the form of an increase in long-term strengths. The binder mixture in the series S85, containing 15 mass% of GGBFS, was found to be the primary binder combination positively impacting the strength development. The obtained results further indicate that replacing 15 mass% of OPC with GGBFS and 5 mass% of MK in the S80 series supported in the majority of samples the development of early strengths within 28 days. However, it should be noted that the presence of GGBFS and MK in the samples resulted in a rise in the strength after 28 and 90 days, respectively, in comparison to the S100 reference. Regarding the impact of the quaternary binder mixture employed in the S65 series, with the replacement of 35 mass% of OPC by 15 mass% of GGBFS, 15 mass% of GL and 5 mass% of MK on the development of compressive strength was lower than that of S85, and S80. The impact of this binder mixture was observed in the long-term strengths. The initial strengths reached lower values than the reference S100.

4.3.5. Shrinkage characteristics

The initial drying of concrete is characterized by a slow increase in strain due to the loss of water released from large capillary pores. Subsequently, an increase in shrinkage rate is observed as a result of the gradual loss of water released from the smaller capillary pores. Hence, in the samples containing a higher portion of capillary pores, there is a potential for a higher shrinkage rate [54]. The shrinkage study results and the results obtained through MIP analysis are consistent with the above claim. The magnetite samples exhibited a lower total porosity when compared to the baryte samples, resulting in a lesser extent of shrinkage.

Regarding the use of fibers, the PP fiber samples exhibited the lowest rate of shrinkage. Compared to the reference, the effect of the steel fibers was evident in the form of a lower shrinkage rate. The shrinkage rate of annual samples according to the type of fibers was reflected in the baryte samples from S100 to S65 as follows: the reference samples reached a range of values of 0.294 to 0.335‰, B-PP from 0.175 to 0.252‰, B-CNT from 0.192 to 0.312 ‰, and B-S from 0.195 to 0.287‰. The magnetite samples M, M-PP, M-CNT, and M-S achieved a range of values between 0.192 and 0.262‰, 0.126 – 0.192‰, 0.182 – 0.223‰, and 0.183 – 0.219‰, respectively.

The influence of the used SCMs was significant, samples with OPC replacement demonstrated lower shrinkage rates. Nonetheless, the exception among analyzed samples was the sample from the S85 series containing GGBFS, displaying the highest shrinkage rate. However, in the samples from the S80 series, containing 15 mass% of GGBFS and 15 mass% of MK, the shrinkage rate dropped below the rate of the reference sample S100.

4.3.6. Pore structure development

The mercury intrusion porosimetry (MIP) was used to characterize the material structure in terms of total porosity, including interparticle, and intraparticle porosity; bulk density; total surface area, as well as pore size distribution. Particular samples from the series S100 and S65 were selected based on their highest compressive strength at each measurement date. From the S100 series, these were samples B-S, and M. From the S65 series, the sample selected was B, except for the 28-day date, where the highest strength was achieved by sample B-S. Furthermore, the samples studied for all the dates were M-S, except 180 days, where the highest strength was achieved by sample M.

According to the MIP analysis results, there was a decreasing trend of total porosity observed in all the samples up to 365 days of curing. Furthermore, it was found that the 2.0 vol.% incorporation of steel fibers increased the total porosity of prepared samples containing both magnetite and baryte aggregates.

In the context of flexural and compressive strength tests, it can be determined that the primary factor influencing the mechanical characteristics of the samples is the total porosity. In addition, it was noted that as the total porosity increased, the compressive strength of the samples decreased.

The influence of aggregates was observed in the series S100 by the higher total porosity of the baryte samples compared to the magnetite samples at all the monitored dates, as well as when comparing the B-S samples from the S100 series with the M-S samples from the S65 series.

According to pore size distribution results is evident that the presence of large capillary pores (0.1 – 10 μm), and macropores (> 10 μm) were increased in the samples containing fibers. This was the most noticeable in the samples with PP fibers. In the S100 and S65 series, significantly higher macropore formation was observed in the combination of PP fibers with baryte aggregate, which occurred to a lesser extent in combination with magnetite aggregate. The impact of aggregate on PSD resulted in a positive effect on the reduction of the volume of all the pore sizes in the samples containing magnetite aggregate. Based on the PSD results it was not possible to determine the influence of SCMs properly. However, based on the literature overview, it could be presumed that the samples with SCMs exhibit a lower volume of capillary pores and macropores. Therefore, the used SCMs demonstrated a positive effect on the pore refinement of FRHWSCCs.

4.3.7. Microstructural analysis

The surface structure of the samples at the microscopic level was investigated in samples from the S100 – S65 series, selected based on the highest achieved compressive strengths after 365 days of curing.

As shown in **Figs. 2 (a)** and **3 (a),** the surface structure of the baryte and magnetite samples differs. On the surface of the baryte samples, there were numerous cavities

in the cement matrix representing defects with possible influence on the mechanical properties. The magnetite samples did not exhibit these cavities.

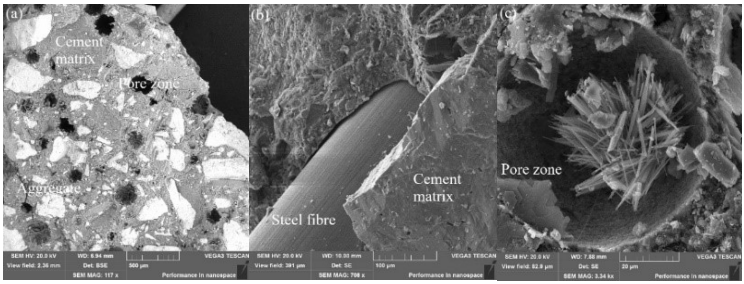

Fig. 2. SEM images of B-S sample from the S100 series.

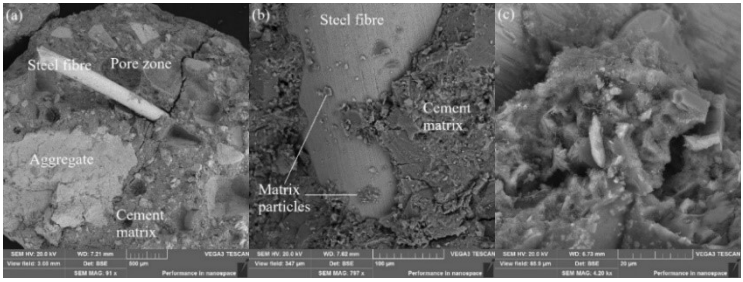

Fig. 3. SEM images of M-S sample from the S85 series.

Figs. 2 (b), and **3 (a)** show the interface between the steel fiber and the cement matrix. A dense structure was observed around the fiber, without the presence of crystalline formations. The occurrence of this structure may explain the relatively high strength values of the samples compared to others and the sufficient adhesion of the fibers to the surroundings [36]. **Fig. 2 (c)** illustrates the needle-like crystals found in one of the pores, with the presumption of AFm phases. In **Fig. 3 (c)**, clusters were observed within the pores, leading to the assumption, that they are in the C-S-H gels [55]. In **Fig. 3 (b)** particles of hydrated cement paste were present on the fiber´s surface, indicating sufficient hydration of the sample.

5. Conclusion

In the present work, the feasibility of designing fiber-reinforced heavyweight self-compacting concrete using baryte and magnetite aggregates, supplementary cementitious materials (GGBFS, GL, and MK); and dispersed reinforcement in the

form of PP, CNT, and S fibers while achieving self-compacting of the mixtures was experimentally verified, with the following key findings:
All the series of prepared FRHWSCC samples possessed the characteristics of SCC concretes and despite the use of heavy-weight aggregate, they did not exhibit any signs of segregation. Depending on the type of fiber used, these samples demonstrated enhanced resistance to tensile stresses in addition to the properties of heavy-weight and self-compacting concretes. Furthermore, depending on the properties observed, the partial replacement of cement by SCMs improved the structural as well as the physicomechanical properties.

References

[1] EFNARC. The European guidelines for self-compacting concrete [online]. 2002. Available from: https://efnarc.org/publications

[2] EFNARC. The European guidelines for self-compacting concrete [online]. 2005. Available from: https://www.theconcreteinitiative.eu/images/ECP_Documents/EuropeanGuidelinesSelfCompactingConcrete.pdf

[3] SHI, C., WU, Z., LV, K.X. and WU, L. A review on mixture design methods for self-compacting concrete. *Construction and Building Materials*. June 2015. Vol. 84, p. 387–398. DOI 10.1016/j.conbuildmat.2015.03.079.

[4] DAUNGWILAILUK, T., YENCHAI, Ch., RUNGJAROENKITI, W., PHEINSUSOM, P., PANWISAWAS, Ch. and PANSUK, W. Use of barite concrete for radiation shielding against gamma-rays and neutrons. *Construction and Building Materials*. April 2022. Vol. 326, art. no. 126838. DOI 10.1016/j.conbuildmat.2022.126838.

[5] GUNOGLU, K. and AKKURT, İ. Radiation shielding properties of concrete containing magnetite. *Progress in Nuclear Energy*. July 2021. Vol. 137, art. no. 103776. DOI 10.1016/j.pnucene.2021.103776.

[6] BAMONTE, P. and GAMBAROVA, P.G. Properties of concrete required in nuclear power plants. *Infrastructure Systems for Nuclear Energy*. 6 December 2013. P. 407–438. DOI 10.1002/9781118536254.ch25.

[7] KARTHIKEYAN, M., ALAN, S., LENIN SUNDAR, M., KUMAR SHARMA, A., VAITHIYANATHAN, V. and SRINIVASAN, K. Load-displacement characteristics of self-compacting steel fiber reinforced concrete beams. *Materials Today: Proceedings*. June 2023. DOI 10.1016/j.matpr.2023.05.557.

[8] GRUYAERT, E., MAES, M. and DE BELIE, N. Performance of BFS concrete: K-value concept versus equivalent performance concept. *Construction and Building Materials*. October 2013. Vol. 47, p. 441–455. DOI 10.1016/j.conbuildmat.2013.05.006.

[9] ZHENG, Ch., WAN, S. and ZONG, Z. Durability evaluation and lifetime prediction of recycled coarse aggregate self-compacting concrete after freeze-thaw and sulfate erosion coupling. *Materials Today Communications*. June 2024. Vol. 39, art. no. 109115. DOI 10.1016/j.mtcomm.2024.109115.

[10] GRDIC, Z.J., TOPLICIC-CURCIC, G.A., DESPOTOVIC, I.M. and RISTIC, N.S. Properties of self-compacting concrete prepared with coarse recycled concrete

aggregate. *Construction and Building Materials*. July 2010. Vol. 24, no. 7, p. 1129–1133. DOI 10.1016/j.conbuildmat.2009.12.029.

[11] ASSAAD, J.J. Influence of recycled aggregates on dynamic/static stability of self-consolidating concrete. *Journal of Sustainable Cement-Based Materials*. 15 January 2017. Vol. 6, no. 6, p. 345–365. DOI 10.1080/21650373.2017.1280427.

[12] CAMPOS, R.S., BARBOSA, M.P., PIMENTEL, L.L. and MACIEL, G. Influência dos agregados reciclados NAS propriedades reológicas E Mecânicas do Concreto autoadensável. *Matéria (Rio de Janeiro)*. 5 March 2018. Vol. 23, no. 1. DOI 10.1590/s1517-707620170001.0300.

[13] FIOL, F., THOMAS, C., MUÑOZ, C., ORTEGA-LÓPEZ, V. and MANSO, J.M. The influence of recycled aggregates from precast elements on the mechanical properties of structural self-compacting concrete. *Construction and Building Materials*. September 2018. Vol. 182, p. 309–323. DOI 10.1016/j.conbuildmat.2018.06.132.

[14] MANZI, S., MAZZOTTI, C. and CHIARA BIGNOZZI, M. Self-compacting concrete with recycled concrete aggregate: Study of the long-term properties. *Construction and* Building Materials. December 2017. Vol. 157, p. 582–590. DOI 10.1016/j.conbuildmat.2017.09.129.

[15] MARTÍNEZ-BARRERA, G., UREÑA-NUÑEZ, F., GENCEL, O. and BROSTOW, W. Mechanical properties of polypropylene-fiber reinforced concrete after gamma irradiation. Composites Part A: Applied Science and Manufacturing. May 2011. Vol. 42, no. 5, p. 567–572. DOI 10.1016/j.compositesa.2011.01.016.

[16] MARTÍNEZ-BARRERA, G., VIGUERAS-SANTIAGO, E., HERNÁNDEZ-LÓPEZ, S., BROSTOW, W. and MENCHACA-CAMPOS, C. Mechanical improvement of concrete by irradiated polypropylene fibers. Polymer Engineering & Science. 2005. Vol. 45, no. 10, p. 1426–1431. DOI 10.1002/pen.20418.

[17] TUFEKCI, M.M. and GOKCE, A. Development of heavyweight high-performance fiber-reinforced cementitious composites (HPFRCC) – part II: X-ray and gamma radiation shielding properties. Construction and Building Materials. February 2018. Vol. 163, p. 326–336. DOI 10.1016/j.conbuildmat.2017.12.086.

[18] MANSOUR, A., MOHYEDDIN, A. and LEE, J. Load-bearing behaviour of anchors in fibre-reinforced concrete – a state of the Art Review. Journal of Building Engineering. August 2024. Vol. 91, art. no. 109580. DOI 10.1016/j.jobe.2024.109580.

[19] DAVIDOVITS, J. Geopolymers. Journal of Thermal Analysis. August 1991. Vol. 37, no. 8, p. 1633–1656. DOI 10.1007/bf01912193.

[20] WEE, T.H., MATSUNAGA, Y., WATANABE, Y. and SAKAI, E. Microstructure and strength properties of high strength concretes containing various mineral admixtures. Cement and Concrete Research. May 1995. Vol. 25, no. 4, p. 715–720. DOI 10.1016/0008-8846(95)00061-g.

[21] ZHAO, Ch., WANG, Z., ZHU, Z., GUO, Q., WU, X. and ZHAO, R. Research on different types of fiber reinforced concrete in recent years: An overview. Construction and Building Materials. February 2023. Vol. 365, art. no. 130075. DOI 10.1016/j.conbuildmat.2022.130075.

[22] WU, Z., SHI, C. and KHAYAT, K.H. Investigation of mechanical properties and shrinkage of ultra-high performance concrete: Influence of steel fiber content and shape. Composites Part B: Engineering. October 2019. Vol. 174, art. no. 107021. DOI 10.1016/j.compositesb.2019.107021.

[23] PENG, S., WU, B., DU, X., ZHAO, Y. and YU, Z. Study on dynamic splitting tensile mechanical properties and microscopic mechanism analysis of steel fiber reinforced concrete. Structures. December 2023. Vol. 58, art. no. 105502. DOI 10.1016/j.istruc.2023.105502.
[24] BANKIR, S. and BIKCE, M. Experimental investigation and statistical evaluation of the effects of steel fiber aspect ratio and fiber rate on static and dynamic mechanical properties of concrete. Construction and Building Materials. February 2024. Vol. 414, art. no. 135064. DOI 10.1016/j.conbuildmat.2024.135064.
[25] YOO, D.-Y., CHUN, B. and KIM, J.-J. Bond performance of abraded arch-type steel fibers in ultra-high-performance concrete. Cement and Concrete Composites. May 2020. Vol. 109, art. no. 103538. DOI 10.1016/j.cemconcomp.2020.103538.
[26] LEE, S.H., KIM, S. and YOO, D.-Y. Hybrid effects of steel fiber and carbon nanotube on self-sensing capability of ultra-high-performance concrete. Construction and Building Materials. October 2018. Vol. 185, p. 530–544. DOI 10.1016/j.conbuildmat.2018.07.071.
[27] YOO, D.-Y., KIM, S., PARK, G.-J., PARK, J.-J. and KIM, S.-W. Effects of fiber shape, aspect ratio, and volume fraction on flexural behavior of ultra-high-performance fiber-reinforced cement composites. Composite Structures. August 2017. Vol. 174, p. 375–388. DOI 10.1016/j.compstruct.2017.04.069.
[28] YOO, D.-Y., KANG, S.-T. and YOON, Y.-S. Effect of fiber length and placement method on flexural behavior, tension-softening curve, and fiber distribution characteristics of UHPFRC. Construction and Building Materials. August 2014. Vol. 64, p. 67–81. DOI 10.1016/j.conbuildmat.2014.04.007.
[29] YANG, L., ZHANG, F., XIE, H., CHEN, S. and LIN, Ch. Dynamic mechanical properties of Red Sandrock-polypropylene fiber reinforced concrete composite under impact load. KSCE Journal of Civil Engineering. 27 December 2021. Vol. 26, no. 3, p. 1479–1493. DOI 10.1007/s12205-021-1233-0.
[30] YANG, T., WANG, S. and LIU, W. Restoring-force model of modified RAC columns with silica fume and hybrid fiber. Journal of Central South University. November 2017. Vol. 24, no. 11, p. 2674–2684. DOI 10.1007/s11771-017-3680-9.
[31] CUI, X., HAN, B., ZHENG, Q., YU, X., DONG, S., ZHANG, L. and OU, J. Mechanical properties and reinforcing mechanisms of cementitious composites with different types of multiwalled carbon nanotubes. Composites Part A: Applied Science and Manufacturing. December 2017. Vol. 103, p. 131–147. DOI 10.1016/j.compositesa.2017.10.001.
[32] ASLANI, F., HAMIDI, F., VALIZADEH, A. and DANG, A.T.-N. High-performance fibre-reinforced heavyweight self-compacting concrete: Analysis of fresh and mechanical properties. Construction and Building Materials. January 2020. Vol. 232, art. no. 117230. DOI 10.1016/j.conbuildmat.2019.117230.
[33] STN EN 1015-11. Methods of test for mortar for masonry. Part 11: Determination of flexural and compressive strength of hardened mortar. ÚNMS SR, 2020. (in Slovak).
[34] STN EN 206/NA. Concrete. Specification, performance, production and conformity. ÚNMS SR. 2021. (in Slovak).
[35] RAHMAN, I.A., VEJAYAKUMARAN, P., SIPAUT, C.S., ISMAIL, J. and CHEE, C.K. Size-dependent physicochemical and optical properties of silica nanoparticles.

Materials Chemistry and Physics. March 2009. Vol. 114, no. 1, p. 328–332. DOI 10.1016/j.matchemphys.2008.09.068.

[36] WEI, B., ZHANG, Y. and BAO, S. Preparation of geopolymers from vanadium tailings by mechanical activation. Construction and Building Materials. August 2017. Vol. 145, art. no. 236–242. DOI 10.1016/j.conbuildmat.2017.03.234.

[37] ABBAS, M.L., ABBAS, W.A. and GÜNEYISI, E. Shrinkage and thermo-mechanical properties of concretes incorporated with different substitutions of natural aggregates by cold bonded calcined attapulgite lightweight aggregates. Journal of Building Engineering. November 2023. Vol. 79, art. no. 107921. DOI 10.1016/j.jobe.2023.107921.

[38] ALLUJAMI, H.M., ABDULKAREEM, M., JASSAM, T.M., AL-MANSOB, R. A., IBRAHIM, A., NG, J.L. and YAM, H.Ch. Mechanical properties of concrete containing recycle concrete aggregates and multi-walled carbon nanotubes under static and dynamic stresses. Case Studies in Construction Materials. December 2022. Vol. 17, art. no. e01651. DOI 10.1016/j.cscm.2022.e01651.

[39] WANG, J., LI, Y., QIU, Z. and ZHANG, Y. Experimental research on compressive properties of recycling polypropylene (pp) fiber recycled coarse aggregate concrete. Journal of Building Engineering. October 2023. Vol. 76, art. no. 107403. DOI 10.1016/j.jobe.2023.107403.

[40] FONSECA, T.V., DOS ANJOS, M.A.S., FERREIRA, R.L.S., BRANCO, F.G. and PEREIRA, L. Evaluation of self-compacting concretes produced with ternary and quaternary blends of different SCM and hydrated-lime. Construction and Building Materials. February 2022. Vol. 320, art. no. 126235. DOI 10.1016/j.conbuildmat.2021.126235.

[41] DRAGOMIROVÁ, J. and PALOU, M. Development of high-compressive heavyweight concrete based on Portland cement and supplementary cementitious materials. Materials Science Forum. 27 May 2019. Vol. 955, p. 44–49. DOI 10.4028/www.scientific.net/msf.955.44.

[42] BARNETT, S.J., ADAM, C.D. and JACKSON, A.R.W. An XRPD profile fitting investigation of the solid solution between Ettringite, CA6Al2(SO4)3(OH)12·26H2O, and Carbonate Ettringite, Ca6Al2(CO3)3(OH)12·26H2O. Cement and Concrete Research. January 2001. Vol. 31, no. 1, p. 13–17. DOI 10.1016/s0008-8846(00)00429-4.

[43] KUZIELOVÁ, E., ŽEMLIČKA, M., MÁSILKO, J. and PALOU, M.T. Effect of additives on the performance of Dyckerhoff Cement, class G, submitted to simulated hydrothermal curing. Journal of Thermal Analysis and Calorimetry. 7 November 2017. Vol. 133, no. 1, p. 63–76. DOI 10.1007/s10973-017-6806-2.

[44] PALOU, Martin T., KUZIELOVÁ, Eva, ŽEMLIČKA, Matúš, BOHÁČ, Martin and NOVOTNÝ, Radoslav. The effect of curing temperature on the hydration of binary Portland Cement. Journal of Thermal Analysis and Calorimetry. 23 March 2016. Vol. 125, no. 3, p. 1301–1310. DOI 10.1007/s10973-016-5395-9.

[45] ROJAS, M.F. and CABRERA, J. The effect of temperature on the hydration rate and stability of the hydration phases of metakaolin–lime–water systems. Cement and Concrete Research. January 2002. Vol. 32, no. 1, p. 133–138. DOI 10.1016/s0008-8846(01)00642-1.

[46] MORSY, M. S. Effect of temperature on hydration kinetics and stability of hydration phases of metakaolin-lime sludge-silica fume system. Ceramics-silikates. 2005. Vol. 4, no. 49, p. 237–241. Available from: https://www.ceramics-silikaty.cz/2005/pdf/2005_04_237.pdf.

[47] SONG, H., JEONG, Y., BAE, S., JUN, Y., YOON, S. and EUN OH, J. A study of thermal decomposition of phases in cementitious systems using HT-XRD and TG. Construction and Building Materials. April 2018. Vol. 169, p. 648–661. DOI 10.1016/j.conbuildmat.2018.03.001.

[48] PACEWSKA, Barbara and WILIŃSKA, Iwona. Usage of supplementary cementitious materials: Advantages and limitations. Journal of Thermal Analysis and Calorimetry. 29 June 2020. Vol. 142, no. 1, p. 371–393. DOI 10.1007/s10973-020-09907-1.

[49] KUZIELOVÁ, Eva, ŽEMLIČKA, Matúš, NOVOTNÝ, Radoslav and PALOU, Martin T. Simultaneous effect of silica fume, metakaolin and ground granulated blast-furnace slag on the hydration of multicomponent cementitious binders. Journal of Thermal Analysis and Calorimetry. 22 October 2018. Vol. 136, no. 4, p. 1527–1537. DOI 10.1007/s10973-018-7813-7.

[50] PONOMAR, V.P. Synthesis and magnetic properties of magnetite prepared by chemical reduction from hematite of various particle sizes. Journal of Alloys and Compounds. April 2018. Vol. 741, p. 28–34. DOI 10.1016/j.jallcom.2018.01.023.

[51] COMINOLI, L., MEDA, A. and PLIZZARI, G.A. Fracture properties of high-strength hybrid fiber-reinforced concrete. Advances in Construction Materials 2007. P. 139–146. DOI 10.1007/978-3-540-72448-3_14.

[52] ÖZTURAN, T. and ÇEÇEN, C. Effect of coarse aggregate type on mechanical properties of concretes with different strengths. Cement and Concrete Research. February 1997. Vol. 27, no. 2, p. 165–170. DOI 10.1016/s0008-8846(97)00006-9.

[53] YAO, X., HAN, Y., SHEN, L. and ZHU, D. Experimental study on the effect of polypropylene fiber on compressive strength and fracture properties of high-strength concrete after elevated temperatures. Journal of Building Engineering. June 2024. Vol. 86, art. no. 108860. DOI 10.1016/j.jobe.2024.108860.

[54] CLAISSE, P. A. Creep, shrinkage, and cracking of concrete. Civil Engineering Materials. 2016. P. 241–249. DOI 10.1016/b978-0-08-100275-9.00023-1.

[55] DUAN, P., SHUI, Z., CHEN, W. and SHEN, Ch. Enhancing microstructure and durability of concrete from ground granulated blast furnace slag and Metakaolin as cement replacement materials. Journal of Materials Research and Technology. January 2013. Vol. 2, no. 1, p. 52–59. DOI 10.1016/j.jmrt.2013.03.010.